EXPERIMENTAL AND COMPUTATIONAL INVESTIGATION OF THE VORTEX FLOW OVER A SWEPT WING

F. Manie[x], M. Néron[xx], V. Schmitt[xxx]

Office National d'Etudes et de Recherches Aérospatiales (ONERA)

92320 CHATILLON France

Abstract

The development of the vortex flow that occurs at the rounded leading edge of the 60° swept rectangular AFV-D wing has been investigated in a wide range of Mach numbers and angles of attack. The important amount of experimental results constitutes a helpful data base for checking advanced computational methods. - At low speeds, the five hole probe surveys give a precise description of the three-dimensional structure of the vortex flow, and, in particular, shows a gradual loss of total pressure in the non-bursted vortex flow. Rehbach's vorticity particles method successfully predicts the mean features of the vortex flow : rolling-up, center line location and velocity field. The present modelling of the vortex shedding process should nevertheless be improved in order to get a better evaluation of the vortex lift. - At transonic velocities, inviscid computations were performed with an Euler code. The wing is ended by a rounded wing tip around which a C-O type grid is built. These first computations seem to show the ability of the method to compute vortex structures, with separation starting from a smooth surface, i.e. here at the leading edge and at the wing tip.

Notation

c	: geometric chord
l	: streamwise chord
b	: wing semi-span
X_v, Y_v, Z_v	: wing triedhral coordinates
V	: velocity
M	: Mach number
P	: static pressure
q	: dynamic pressure
pt	: total pressure
C_p	: static pressure coefficient $C_p = \frac{P - P_o}{q_o}$
C_{pt}	: total pressure coefficient $C_{p_t} = \frac{P_t - P_o}{q_o}$
Re_l	: streamwise Reynolds number
α	: angle of attack
φ	: wing sweep angle
$\vec{\omega}$	: vorticity vector

Subscript

o	: freestream

x Research Engineer, Applied Aerodynamics

xx Research Scientist, Theoretical Aerodynamics

xxx Senior Research Engineer, Applied Aerodynamics

I. Introduction

For several years intensive efforts have been devoted in many countries to high-angle-of-attack aerodynamics [1,2]. This trend is strongly related to demands of performance and manoeuvrability on modern fighter-aircrafts and missiles, which exhibit various types of vortical flow at high angle of attack. As far as slender wings are concerned, the main topics of interest are the improvement of knowledge of leading edge vortex flows and also the development of prediction methods for design purposes. On the one hand indeed recent experimental studies have been concerned with flow field surveys in order to investigate such problems as vortex structures, stability and breakdown [3,4]. On the other hand panel methods including various vortex modelling [5,6] and more recently Euler methods [7,8] have been used to predict such types of flows and to assess their aptitude as a tool for designers.

Both subjects are also investigated at ONERA especially on a very simple rectangular wing that is characterized by a 60° sweep angle and a rounded leading edge. Wind tunnel tests have been conducted during recent years on this so-called AFV-D wing, not only at a 60° sweep angle but also at other sweep angles, from low speeds to the transonic regime. Very first results mainly based on force measurements, wing pressure distributions and flow visualisations were reported in a previous ICAS paper [9].

The present work is focused at low speeds on flow field investigations provided by wind tunnel tests by means of a five hole pressure probe and computations with Rehbach's unsteady "vorticity particles" method [10] in order to assess them. In the transonic domain it deals with first computations of flows on the AFV-D wing at 60° sweep angle by means of a pseudo-unsteady Euler approach [11]. The basic aim of these attempts was to verify the capability of this method to give solutions including leading edge separations, even in the case of a smooth surface such as a rounded leading edge.

This work was partly supported by the French Government Service D.R.E.T. (Direction des Recherches, Etudes et Techniques).

II. Low speed vortex flow over the AFV-D wing

II.1 General features

A general view of the set-up on the wall in the F1 pressurized wind tunnel (fig. 1a) shows the half-model set on a boundary layer diverter. The special device for flow field surveys is visible in the background. The model geometry and pressure hole locations on the upper surface are indicated on figure 1b. More details on this model and its basic ONERA-D profile (symmetrical, leading edge radius r/c = 0.0143) can be found in [12].

At low speeds vortical flow is generated on the AFV-D wing within a large range of angles of attack going from α_a = 5° to 12°. This angle is characterized by a typical growth of the lift slope. It depends strongly on the Reynolds number as depicted in figure 2. Beyond a "critical" Reynolds number the formation of the leading edge vortex is delayed to rather high angles of attack. This behaviour has been related [13] to the type of the laminar separation bubble that occurs at very low angles of attack on this wing. At low Reynolds numbers the bubble is "long" and is directly at the origin of the vortical flow generation, whereas such an influence cannot be noted at high Reynolds numbers, when the bubble is "short". These remarks are relevant for wings with rounded leading edges. When the leading edge is sharp, vortical flows appear independently of the Reynolds number at very low angles of attack.

With the increase of the angle of attack the leading edge vortex flow continuously develops over the wing until the appearance of breakdown effects at the side edge for an angle of attack α_b. Opposite to α_a, the corresponding angle of attack α_b does not vary significantly with the Reynolds number, at least in the investigated range $1 \times 10 \leqslant Re_1 \leqslant 5 \times 10^6$.
By further increase of the angle of attack the breakdown point moves forward to the wing apex as shown in figure 3. This curve is deduced from the pressure distributions measured on the upper surface on the wing. More precisely, in a first approach vortex breakdown is considered to reach a given section at the minimum value of Cp_{min} versus α .

Finally, the maximum lift C_{Lmax} of the AFV-D wing is obtained at an angle of attack of about 30°.

It is obvious that force and pressure measurements or wall streamline visualisations are not sufficient to determine the characteristics of flows generated by a leading edge separation. More quantitative information is therefore needed in the whole flow field on the one hand for analysing vortical flow development and structures and on the other hand for assessing computational methods.

The flow field investigation methods which have been developed by ONERA for the F1 tunnel and other large wind tunnels are described in [14]. They are based on the use of a special motorized exploring device allowing flow surveys in a part of the test section. In the particular case of the AFV-D wing tests it generated large spherical surfaces that may be assimilated to planes which are quasi-perpendicular to the freestream velocity. Measurements were made by means of a five hole pressure probe providing mean values of the velocity vector as well as local static and total pressure coefficients. As the flow direction in a vortical flow strongly varies, several orientations of the probe are needed in order to improve the probe efficiency. This type of measurement may, however, fail in a bursted vortex core, where the velocity is very small and even becomes negative. In order to alleviate the cost of such tests a computer controlled piloting procedure [15] was used.

The flow surveys on the AFV-D wing were mainly performed at a freestream velocity V_o = 40 m/s . An upper surface pressure distribution analysis led to the choice of three angles of attack α = 13°, 19° and 24° for which the vortex breakdown is respectively located beyond the wing tip, at mid-span and near the apex. The corresponding pressure distributions are shown on figure 4 as isobar contour lines. The vortex breakdown have also been sketched in this figure.

For the discussion only some flow field results were selected. They were obtained mainly in the mid plane that intersects the wing root at the trailing edge, and also in an upstream and a downstream plane respectively situated in the apex and the wing tip region (see also sketch of fig. 12). A primary representation of probe surveys is a plane projection of the local velocity vector measured in the mid plane and plotted at α = 13°; 19° and 24° in figure 5. This representation leads to a first evaluation of the vortex strength and of its core location. In particular the lack of measurements in the vortex core at α = 19° and 24° is mainly due to breakdown effects.

More information is provided by contour lines such isovelocity ($\overline{V}$ modulus = V) and isobar (Cp_t=pressure coefficient) curves. At α = 13°, still before the appearance of vortex breakdown, the velocity contours (fig. 6a) present a typical structure which exhibits an overvelocity zone above a subvelocity zone. This corresponds to the superposition of the vortical and of the transverse flow fields. The locus of the maximum determines then the outer limit of the phenomenon whereas the minimum defines the core. These geometrical characteristics agree with those that come out from the isobar contours of figure 6b. They clearly demonstrate (Cp_t = 1) the non circular feature and the extension of the vortex. The curves moreover reveal the gradual loss of total pressure in the core. These characteristics distinguish in fact vortex flows on wings with moderate high sweep angles and rounded leading edges from sharp edged slender wing vortices. These indeed present a much more concentrated total pressure loss in their core [16,17] .

The flow survey in the same mid plane at α = 19° shown in figure 7 is particularly interesting. On the one hand it may be close to the vortex breakdown location (see fig. 4) ; this is proved by the very low velocity level and the deep total pressure loss which were measured in the center : $V/V_o \simeq 0.4$ and $Cp_t \simeq -2.3$. On the

other hand, the change of the flow structure occurring upstream of the primary vortex ($Y_v/c \simeq 1.1$) may correspond to a secondary vortical flow which is contrarotative.

This kind of flow survey gives very complete information about vortical flows. However, the intrusive method used might perturb the flow locally. Only three-dimensional LDV techniques can corroborate the present results. However, they should open access to the region close to the leading edge and therefore provide useful insights into the initial conditons of the vortex flow with a view to improve their modelling to be used in the prediction method which is described in the next section.

II.2 The vorticity particles method

The theoretical background and the numerical treatment of this method have been reported in some detail in [10]. Only broad outlines will be recalled here.

In a domain (D) surrounding the surface (S) one considers an incompressible inviscid flow. It is described in terms of a vorticity distribution defined by

$$\bar{\omega} = \nabla \times \bar{V} \qquad (2.1)$$

$\bar{V}$ being the velocity vector. In a time dependent approach using Lagrangian variables, vorticity loaded fluid particles are shed into the flow field from separation lines on (S). Their time dependent evolution is governed by the Helmholtz equation

$$\frac{D\bar{\omega}}{Dt} = (\bar{\omega} \cdot \nabla)\ \bar{V} \qquad (2.2)$$

The local velocity $\bar{V}$ due to the vorticity distribution in (D) and on the solid surface (S) in a flow field with the uniform velocity V_o can be expressed employing Green's identity

$$\bar{V} = \bar{V}_o + \frac{1}{4\pi}\iiint_D \left(\operatorname{grad}\frac{1}{r}\right)\times\bar{\omega}\,d\delta + \frac{1}{\pi}\iint_S \left(\operatorname{grad}\frac{1}{r}\right)\times\left(\bar{\xi}\times\bar{V}\right)d\sigma \qquad (2.3.)$$

where $r = |\bar{r}|$ and $\bar{\xi}$ is the outward unit normal to the surface (S).

The calculation method consists in following the motion of a limited number of vorticity particles which leave in the present approach the lifting surface at points distributed on its edges. It is emphasized here that the construction of a spatial grid is not required. The lifting surface is discretized by plane panels using doublet distributions of constant strength for each panel. The vortex shedding mechanism employed is derived from Kutta-condition type considerations.

At each time step new vorticity particles leave the lifting surface. All particles having the same origin instantaneously belong to an emission line which, as long as the flow is unsteady, is not a streamline, a vortex line nor a trajectory.

Taking into account former encouraging results obtained on very various geometric shapes [18,19] the basic numerical treatment has been improved in order to ensure more robustness and better computational performance. This leads now to finer meshes and more emission lines that are required for an assessment of the method.

For the present computations the panelling of the AFV-D wing as a zero thickness lifting surface with the actual wing planform is depicted in figure 8. This surface is discretized by 120 panels and 22 particle shedding points are defined on the edges including 12 points on the leading edge. All computations related in the next section were performed on a Cyber 170-750 and needed 50 to 80 time steps up to a converged lift level.

II.3 Computational and experimental results

In order to illustrate the versability of the method at first two calculations have been performed, the angle of attack of the wing being $\alpha = 19°$. In the one case vorticity particles are shed into the flow field only on the trailing edge and the side edge, whereas in the other case the leading edge in addition is concerned. The respective emission lines of figure 9 corresponding to converged solutions reveal remarkable differences. In the first solution indeed the vortex sheet is a typical one for attached flow ; the weak roll-up at the side edge may be explained by the cropped shape of the wing tip. In the second one a well organized leading edge vortex flow spreading out the whole wing is predicted. There is no doubt that it represents an interesting simulation of such leading edge separation effects.

Concerning the latter computation the time dependent evolution of the normal force coefficient is shown in figure 10. After 60 time steps a nearly converged solution is obtained. It has to be noted here however, that the predicted value underestimates the experimental result of about 10%. This point will be discussed later on.

With further computations of leading edge separations at $\alpha = 13°$ and $24°$ it is possible to analyse the flow development when the angle of attack increases. As converged solutions are concerned, streamlines can be calculated in the whole flow field independently of the basic emission lines. Figure 11 illustrates such results for $\alpha = 13°$, $19°$ and $24°$. When increasing the angle of attack, the vortical flow as expected separates more and more from the lifting surface and progressively turns to the symmetry plane. Of course, all these computations were performed with the same parameters such as grid, time step or vortex shedding mechanism i.e. so reliable results were obtained.

Some comparisons with the above described flow measurements are made at $\alpha = 19°$. Computational and experimental velocity vectors in the three selected cross-planes reveal (fig. 12) a qualitative good agreement of the respective vortical flows. In particular, very similar vortex core locations have to be noted. In spite of some differences in the magnitudes the calculated and measured velocity contours in the mid-span plane shown on figure 13 corroborate this statement. Nevertheless, certain discrepancies are found when comparing both pressure fields on the wing resulting in small differences in the lift coefficient as already mentioned before. Of course, these discrepancies may be explained

by the assumption of a zero thickness sharp edged wing and a rather coarse grid used in the computation, but it is thought that the present modelling of the vortex shedding process requires assessment, at least when leading edge separation occurs. Further investigations in this field are felt to be very important.

III. Transonic flows

Experiments have been made on the same model in the transonic test section of the S2MA wind tunnel in the ONERA center at Modane. These tests covered a Mach number range from 0.275 to 1.2 for angles of attack from 0° to 32°. The measurements included overall forces, pressure distributions on the wing and visualisations of the wall flow by a dye technique. The results have been discussed in some detail in a previous paper [20].

In this work, emphasis is mainly laid on the capabilities of steady inviscid flow calculations using the Euler equations to model transonic flows, possibly including separations, in this particular case of a highly swept wing with a rounded leading edge, at different angles of attack.

The "H" pseudo-unsteady method used here for solving the Euler equations with the isoenergetic assumption, has been developed at ONERA for various applications including 3-D cases (nozzles, rotor cascades, blunt body flows) [21,22,23]. More recently, it has been extended to the computations of flows past wings, as a result of a cooperation between MATRA and ONERA [24,11]. This method permits computing weak solutions of the steady Euler equations, with shocks and vortex sheets, in the case of isoenergetic flows [11]. This property of the Euler equations has allowed them to be used by several authors, especially for flows with vortex sheets [25] including flows with separation at the leading edge [26,27,28].

A key question is: which types of separations is such a method able to predict, and in particular, is it able to capture vortex sheets leaving a smooth surface, for example here the rounded leading edge of the AFV-D wing at a 60° sweep angle.

In the case of such a wing, and from a practical point of view, another question is whether or not, and in the affirmative how, vortical flows are generated at various angles of attack.

After a short presentation of the computational method, including the grid generation and the calculation procedure, the results for three test cases are compared with the experiments.

III.1 The "H" pseudo-unsteady method for solving the steady Euler equations

- Equations and numerical scheme

The total enthalpy H being assumed to be constant, the system of equations is simply composed of the unsteady continuity and momentum equations (3.1), in which the pressure p is a function of the density ρ and the velocity $\bar{V}$, through Bernoulli's relation (3.1 c).

$$\frac{\partial \rho}{\partial t} + \operatorname{div} \rho \bar{V} = 0 \qquad (3.1a)$$

$$\frac{\partial \rho \bar{V}}{\partial t} + \overline{\operatorname{div}}\left(\rho \bar{V} \otimes \bar{V} + p \bar{\bar{I}}\right) = \bar{0} \qquad (3.1b)$$

$$p(\rho, \rho \bar{V}) = \frac{\gamma-1}{\gamma}\left[\rho H - \frac{1}{2}\frac{(\rho \bar{V})^2}{\rho}\right] \qquad (3.1c)$$

The replacement of the unsteady energy equation by (3.1c) allows a reduction of the number of the scalar equations from 5 to 4, and therefore, a reduction of the computational cost. The pseudo-unsteady system (3.1), which can be written :

$$\frac{\partial f}{\partial t} + \frac{\partial F_\ell}{\partial x_\ell} = 0 \qquad (3.2)$$

is integrated step by step with respect to time, by means of an explicit predictor-corrector finite-difference scheme, derived from the MacCormack scheme, the discretization of the equations being performed directly in the physical space, using an arbitrary curvilinear mesh [21]. The predictor $\tilde{f}^{n+1}$ and the corrector $f^{(n+1)_c}$ are computed by :

$$\begin{aligned} \tilde{f}^{n+1} &= f^n - \Delta t\left[\delta_\ell^+ F_\ell(f^n)\right] \\ f^{(n+1)_c} &= f^n - \frac{\Delta t}{2}\left[\delta_\ell^+ F_\ell(f^n)\right] - \frac{\Delta t}{2}\left[\delta_\ell^- F_\ell(\tilde{f}^{n+1})\right] \end{aligned} \qquad (3.3)$$

where δ_ℓ^+ and δ_ℓ^- are the forward and backward finite difference operators relative to each index ℓ [22].

- Artificial viscosity terms

The artificial viscosity terms which are added after the computation of the corrector in order to insure the stability of the solution, are composed of a non-linear second order term D^2 and a linear fourth order term D^4 :

$$f^{n+1} = f^{(n+1)_c} + D^2(f^n) + D^4(f^n)$$

The fourth order term D^4 is given, for one dimension, by :

$$D^4(f) = \mu_0\left[f_{i+2} - 4 f_{i+1} + 6 f_i - 4 f_{i-1} + f_{i-2}\right] \qquad (3.4)$$

for $f = (\rho, \rho u, \rho v, \rho w)$. The second order term D^2, which is expressed for one dimension, by :

$$D^2(f) = \mu_1\left[+\frac{\rho_i+\rho_{i+1}}{2}\left|g_{i+1}-g_i\right|\left(g_{i+1}-g_i\right) - \frac{\rho_i+\rho_{i-1}}{2}\left|g_i-g_{i-1}\right|\left(g_i-g_{i-1}\right)\right] \qquad (3.5)$$

for g = (0, u, v, w), is obtained from : $\frac{\partial}{\partial x}\left(\rho\left|\frac{\partial g}{\partial x}\right|\frac{\partial g}{\partial x}\right)$, when discretized in cartesian coordinates, in a uniform mesh.

- Boundary conditions

The boundary conditions, as well as the matching condition between the upper and lower half-spaces, are treated using the compatibility relation theory. The properties of the pseudo-unsteady system (hyperbolicity, compatibility relations, and characteristic cone) were presented in 2-D in [21] and in 3-D in [22,11]. The three specified conditions at the upstream boundary are the velocity direction (two conditions) and the total pressure. At the downstream boundary, a "non reflecting condition" which is an extension of the one proposed in 1-D by HEDSTROM [29] is used. On the wall, as well as on the symmetry plane, the following simple slip condition is used : $\bar{V} \cdot \bar{\xi} = 0$, $\bar{\xi}$ being the unit outward normal to the boundary. Let us note that there is no special treatment at the trailing edge.

- Local time step technique

A local time step technique is used, the time step Δt at the current point being computed from a maximal value, Δt_{max}, obtained by the local C.F.L. criterion, $\Delta t = C_t \cdot \Delta t_{max}$, where C_t is an empirical safety factor (C_t= 0.8). This technique allows important computing time savings, the time steps not being limited by the size of the smallest mesh cell. This limitation would be especially severe here, because of the small mesh cells used near the wing tip.

- Grid generation

One of the difficulties encountered in the computations of 3-D flows past a wing is related to the modelling of the flow around the wing tip. In order to make a detailed numerical study of the flow passing around the wing tip, a rounded wing tip and a mesh of C-O type have been used for the computation (fig. 14). In spite of the highly sweep angle (60°) of the wing, a simple choice for the mesh on the wing consisted in constant-J lines parallel to the vertical symmetry plane, and constant-I lines mainly parallel to the leading edge and to the trailing edge (fig. 15). The constant-I and constant-J surfaces turn respectively around the leading edge and the tip (fig. 16). As the basic numerical scheme is non symmetric, the discretizations of this scheme used in the upper and lower half-meshes, on each side of the horizontal cut half-plane, were chosen symmetrical of one another. A 51 x 50 x 17 mesh has been used, with 36 x 50 points on the wing.

- Calculation procedure

For the present calculations, the code was implemented on a CRAY-1 computer. These very first calculations obtained with this code on this 60° swept AFV-D wing were performed at a Mach number M = 0.92. First, the non-lifting case (α= 0°) was computed, the flow being initialy uniform. After 4000 iterations, the mean residual values $\frac{1}{N}\sum\frac{1}{\Delta t}\left|\rho^{n+1}-\rho^{n}\right|$ were lower than 1.5 10^{-4}. This solution was used to initialize the next computation at α = 4°, the angle of attack increasing first from α = 0° to α= 4° in 2000 iterations, and next remaining constant during 4000 iterations, the mean residual values reaching then 1.8 10^{-4}. Again, this last solution was used to obtain an initial field at α= 6°, α increasing from α = 4° to α= 6° in 1000 iterations. But the computation performed at α= 6° stopped after 1059 iterations, because of a local problem of overvelocities appearing at the wing tip, a few points ahead of the trailing edge. The mesh in this downstream part of the wing tip region, near the trailing edge, appears to be insufficient, at the wall and around it, to model correctly the passing of the flow round the wing tip. However, it seemed interesting to present the solution obtained after 1000 iterations at α= 6°, yet not converged, the mean residual values being about 5.10^{-2}, as a new type of flow seems to occur at this angle of attack.

III.2 Comparison between experimental and computational results

In order to facilitate the discussion of this comparison, it seems to be helpful to give first a short review of the main features of the flow occurring in the wind tunnel tests at a Mach number M_o = 0.92 by increasing the angle of attack from 0° up to $\alpha(C_{L_{max}})$. At this Mach number, the behaviour of the flow does not basically differ from that observed at low speeds. So, at α= 0° the flow remains mainly two-dimensional and subcritical. Due to its shape the leading edge exhibits a small suction peak. This peak becomes more pronounced when the angle of attack increases, and generates both a separation bubble (at α= 1.5°) and a shock wave. When the shock is strong enough to cause the separation of the boundary layer, the formation of a vortical flow can be observed. At a Reynolds number of Re_1 = 2.3 x 10^6, this regime appears at α = 4.5°. As shown in [20] the vortex whose origin is located at the wing apex quickly grows, producing its non-linear effects on the C_L-curve. Then the vortex breakdown starts to affect the pressure field of the upper surface at α= 12° and finally the C_{Lmax} is reached at α= 25°.

Let us now compare some experimental and numerical results in the available test cases.

In the non-lifting case (α = 0°), the comparison of the iso-p/p_{to} lines on the wing (fig. 17) shows a good agreement between computation and experiment, in spite of the difference of the wing planforms. At this angle of attack, the flow is mainly spanwise constant. The pressure distributions in the wing section 7, the mid-span, perpendicular to the leading edge, confirms this good agreement (fig. 18).

At α = 4°, the flow is slightly supersonic in a large region, on the upper surface, both in the computation and in the experiment. The comparison of the iso-p/p_{to} lines shows a relatively good agreement on most part of the upper surface (fig. 19), downstream of the first 15% of the local chord. On the whole, the flow remains mainly spanwise constant. More precisely, it can be noticed that the isobar lines are not exactly parallel to the constant chord line, but get slightly nearer to the leading edge in the outer part of the wing. However, great differences appear in the experimental and numerical flows in the first 15% of the local chord, as it can be observed on the pressure distributions obtained in two sections of the wing, respectively for the sections 5 and 9 (fig. 20). The suction peak observed at the leading edge, which increases in the spanwise direction is much less important in the experiment than in the computation, in which it is associated to a highly supersonic region (M≃2 to 2.5), limited downstream by a relatively strong shock. In the experiment, the adverse pressure gradient behind the suction peak generates a separation bubble which leads to a little plateau which is more extended in the outer part of the wing. Of course, the inability of inviscid flow calculations to predict strongly interacting viscous effects such as those due to a separation bubble, brings a limit to such comparisons with experiment. On figure 21, the planar views of the computed velocity at the points of two constant-I mesh surfaces, one at the trailing edge and one downstream, show the tip vortex, which is enhanced in the computation by the planform of the wing.

When increasing the angle of attack from $\alpha = 4°$ to $\alpha = 6°$, the flow features change, but much more in the experiment than in the computation. It is recalled that this computation has not converged, but has been interrupted, as was explained in III.1

An important change of the pressure field can be noted on the experimental isobar lines (fig. 22) which corresponds to the appearance at the leading edge of the vortical flow already described. On the same figure, the evolution of the computational flow is less important. On the pressure distributions in the same sections as previously (fig. 23), the experimental results present the typical shapes due to a leading edge vortex, the suction peaks having vanished. On the contrary in the computation, the suction peak due to the supersonic region is still present. However, in the outer section, a small region in which the flow is reaccelerated can be noticed downstream of the suction peak, which might indicate a change of the type of flow.

Indeed, the visualisations of the computed velocity field show the presence of a vortical flow, just downstream of the suction peak region, on the outer half of the wing (fig. 24, 25 and 26). The flow field on two constant-I grid surfaces (fig. 24), one just downstream of the shock and the other at half-chord, show the vortex and the thin layer near the wall in which the fluid moves towards the tip. The separation of the flow passing round the wing tip can be seen on these figures.

On figure 25 are compared the velocity fields on the wing upper surface, computed at both angles of attack $\alpha = 4°$ and $\alpha = 6°$. This comparison shows clearly the beginning flow transformation. On figure 26 are represented for both cases the velocity fields on the J = 13 grid-surface, viewed in a direction parallel to the leading edge or trailing edge. The vortical flow can easily be observed, for $\alpha = 6°$, the separation beginning one or two points downstream of the shock.

Thus, although quite different from the experiment, this preliminary result seems to demonstrate the capability of the Euler approach to model without any special treatment separations on smooth surfaces such as, in this particular case, vortical flows on a rounded leading edge.

IV. Conclusions

In order to improve the knowledge of vortical flows which occur on the leading edge of swept wings, ONERA has devoted great efforts for several years. One of the main supports used is a very simple rectangular variable swept wing with a rounded leading edge, the AFV-D wing studied here at a 60° sweep angle.

Low speed tests on this wing exhibit a strong Reynolds number influence on the formation of the vortical flow which occurs in a quite large domain of angle of attack.

This result is mainly related to the large leading edge radius of the model. Investigations by means of a five hole pressure probe provide useful insights in the vortex structure. Due to the wing shape, noticeable differences with classical delta wing vortices appear in the flow field, even upstream of the vortex breakdown. Such a data base is also a helpful tool to check computational methods. Concerning this field two theoretical approaches have been used.

First, with a thin wing discretization of the actual configuration, the great capabilities of Rehbach's unsteady vorticity particles method are demonstrated in some low speed cases. Solutions show a qualitatively good agreement with various vortex sheets observed on the wing. Nevertheless, it clearly appears that they depend more or less strongly on the initial conditions of the vorticity vectors for which more knowledge is needed.

Secondly, at transonic regime, the "H" pseudo-unsteady method for solving the Euler equations was used for computations on a wing with the same thickness as in the experiment, but with a modified planform. At $\alpha = 4°$, the importance of the viscous effects, with the presence of a separation bubble, seems to bring a limit to the interest of the experiment-computation comparison.

One of the main purposes of this study was to test the method ability to capture separation starting from a smooth surface. The computation performed at $\alpha = 6°$ presents two types of limitations. Firstly, it was not converged. Secondly, a leading edge supersonic region was observed in this computation which does not exist in the experiment. It must be noted that these computations were performed from initial conditions obtained from solutions at the same Mach number, by increasing the angle of attack. Another way to proceed would consist in gradually increasing the Mach number from a solution obtained at the same angle of attack, but at subsonic velocities. It is not sure that the latter way of proceeding, which has to be tested, will lead to the same type of solution, with a supersonic region at the leading edge. However, in spite of its limitations, the present calculation at $\alpha = 6°$ seems to indicate that the method would be able to compute a vortex structure starting from a rounded leading edge.

References

1 "High Angle of Attack Aerodynamics". AGARD Conference Proceedings n° 247.

2 "Aerodynamics of Vortical Type Flows in Three Dimensions". AGARD Conference Proceedings n° 342.

3 HUMMEL, D., "On the Vortex Formation over a Slender Wings at Large Angles of Incidence". AGARD C.P. 247, 1978.

4 SOLIGNAC, J.L. and LEUCHTER, O., "Etudes expérimentales d'écoulements tourbillonnaires soumis à des effets de gradient de pression adverse". AGARD C.P. 342, 1983.

5 SMITH, J.H.B., "Theoretical Modelling of Three Dimensional Vortex Flows in Aerodynamics". AGARD C.P. 342, 1983.

6 HOEIJMAKERS, H.W.M., "Computational Vortex Flow Aerodynamics". AGARD C.P. 342, 1983.

7 ERIKSSON, L.E. and RIZZI A., "Computation of Vortex Flow Around Wings Using the Euler Equations". Ed. H. VIVIAND, Proc. IVth GAMM Conf. Num. Meth., Vieweg Verlag, 1982.

8 HITZEL, S.M. and SCHMIDT, W., "Slender Wings with Leading-Edge Vortex Separation. A Challenge for Panel-Methods and Euler Codes". AIAA paper 83-0562.

9 MANIE, F., REHBACH, C. and SCHMITT, V., "Etude d'une aile à flèche variable en écoulement sub ou transsonique." ICAS, Lisbonne, 1978.

10 REHBACH, C., "Numerical Calculation of Three-Dimensional Unsteady Flows with Vortex Sheets". AIAA paper 78-111.

11 NÉRON, M. and KOECK, C., "Computations of Three-Dimensional Transonic Inviscid Flows on a Wing by Pseudo-Unsteady Resolution of the Euler Equations". Eds. M. PANDOLFI, R. PIVA, Proceedings Vth GAMM Conf. Num. Meth., Vieweg Verlag, 1984.

12 MANIE, F. and RAYNAL, J.C., "Transonic Measurements on the - ONERA AFV-D - Variable Sweep Wing in the - ONERA S2MA - Wind Tunnel". AGARD A.R. 138, 1979.

13 BROCARD, Y. and MANIE, F., "Etudes des caractéristiques de l'écoulement tourbillonnaire sur une aile en flèche". L'Aéronautique et l'Astronautique n° 82, 1980.

14 BROCARD, Y. and DESPLAS, PH., "Méthodes d'exploration des écoulements tourbillonnaires développées pour la soufflerie F1". AGARD C.P. 348, 1984.

15 BROUSSAUD, P., "Dispositif pour l'étude détaillée de l'écoulement autour de grandes maquettes en soufflerie". 60th Meeting S.T.A., Williamsburg, 1983.

16 HUMMEL, D., "Untersuchungen über das Aufplatzen der Wirbel an schlanken Deltaflügeln". Z. Flugwiss. 13, 1965.

17 FINK, P.T. and TAYLOR, J., "Some Low Speed Experiments with 20 deg. Delta Wings". R M n° 3489, Part II, 1967.

18 CHOMETON, F., "Calculs d'écoulements tridimensionnels décollés autour de véhicules terrestres". 18ème Colloque AAAF, Poitiers, 1981.

19 BOSCHIERO, M., "Calculs de structures tourbillonnaires tridimensionnelles autour de missiles". 18ème Colloque AAAF, Poitiers, 1981.

20 BROCARD, Y. and SCHMITT, V., "Interaction aérodynamique entre un canard proche et une aile en flèche en écoulement transsonique". AGARD C.P. 285, 1980.

21 VIVIAND, H. and VEUILLOT, J.P., "Méthodes pseudo-instationnaires pour le calcul d'écoulements transsoniques". ONERA, Publication n° 1978-4 (English translation : ESA-TT 561).

22 BROCHET, J., "Calcul numérique d'écoulements internes tridimensionnels transsoniques". La Recherche Aérospatiale pp. 301-315, n° 1980-5 (English Translation ESA-TT 673).

23 ENSELME, M., GUIRAUD, D. and BOISSEAU J.P., "Contribution à l'évaluation de l'intérêt de calculateurs à structure parallèle pour la résolution de systèmes d'équations aux dérivées partielles". ONERA T.P. 1980-160.

24 CHATTOT, J.J., BOSCHIERO, M. and KOECK, C., "Méthodes numériques de prédiction de l'aérodynamique des missiles". AGARD C.P. 336, 1982.

25 ERIKSSON, L.E. and RIZZI, A., "Computations of Vortex Flow Around a Canard-Delta Combination". Eds. M. PANDOLFI, R. PIVA. Proceedings of the Vth GAMM Conference on Numerical Methods in Fluid Mechanics. Vieweg-Verlag, 1984.

26 RIZZI, A. and ERIKSSON, L.E., "Entropy Production and Vortex-Sheet Capturing in Numerical Solutions of the Euler Equations", INRIA Workshop on Numerical Methods for the Euler Equations. Rocquencourt, France, 7-9 décembre, 1983.

27 RIZZI, A., ERIKSSON, L.E., SCHMIDT, W. and HITZEL, S., "Numerical Solution of the Euler Equations Simulating Vortex Flow Around Wings". AGARD C.P. 342, 1983.

28 RAJ, P. and SIKORA, J.S., "Free-Vortex Flows : Recent Encounters with an Euler Code". AIAA paper 84-0135, 1984.

29 HEDSTROM, G.W., "Non-Reflecting Boundary Conditions for Non Linear-Hyperbolic Systems". J. of Comp. Physics n° 39, 1979.

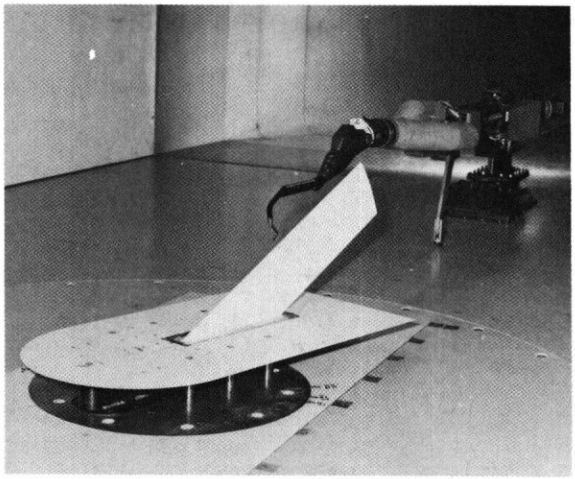

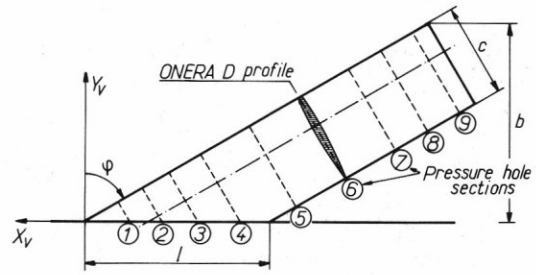

$c = 0.2m$
$l = 0.4m$
$b = 0.43m$

Fig. 1 - AFV-D wing model
a. set-up in the wall in the F1 wind tunnel.
b. wing geometry and pressure hole distribution.

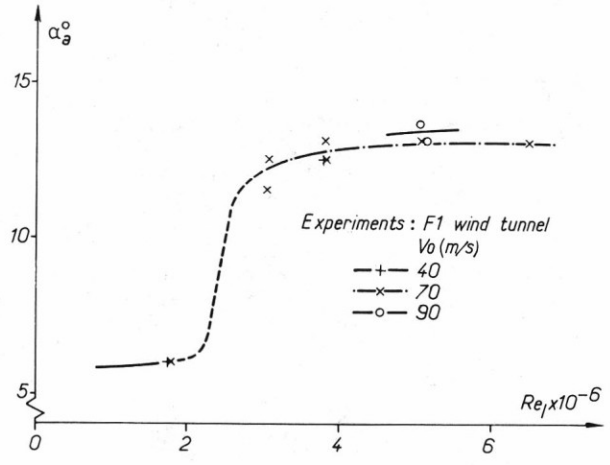

Fig. 2 - Appearance of leading edge vortex flow on the wing.

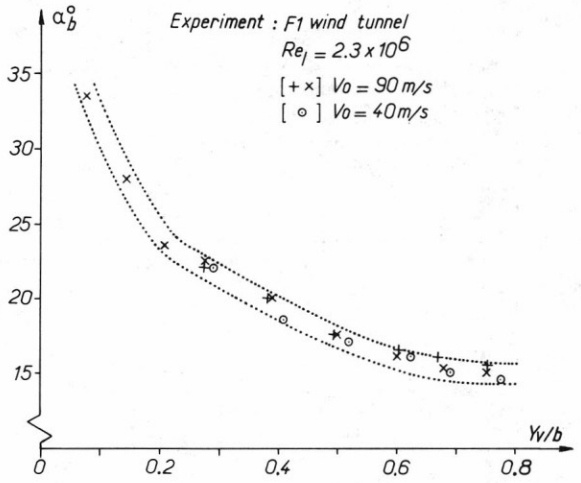

Fig. 3 - Vortex breakdown evolution on the upper surface.

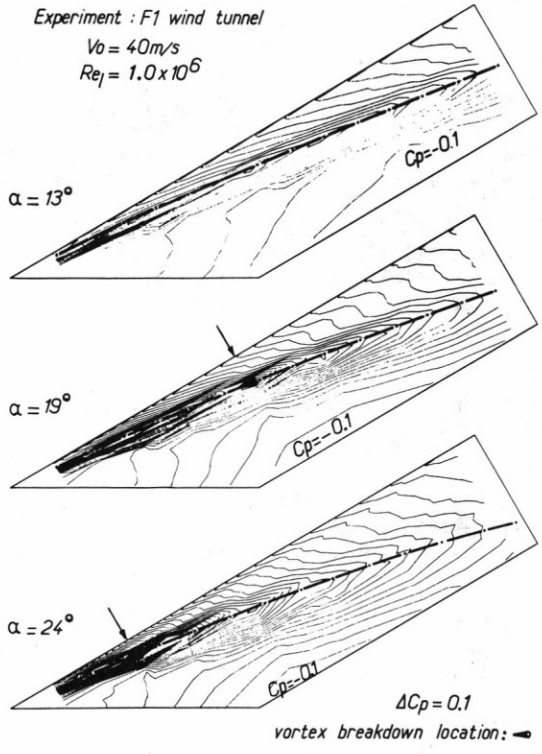

Fig. 4 - Upper surface isobar contour lines at various angles of attack.

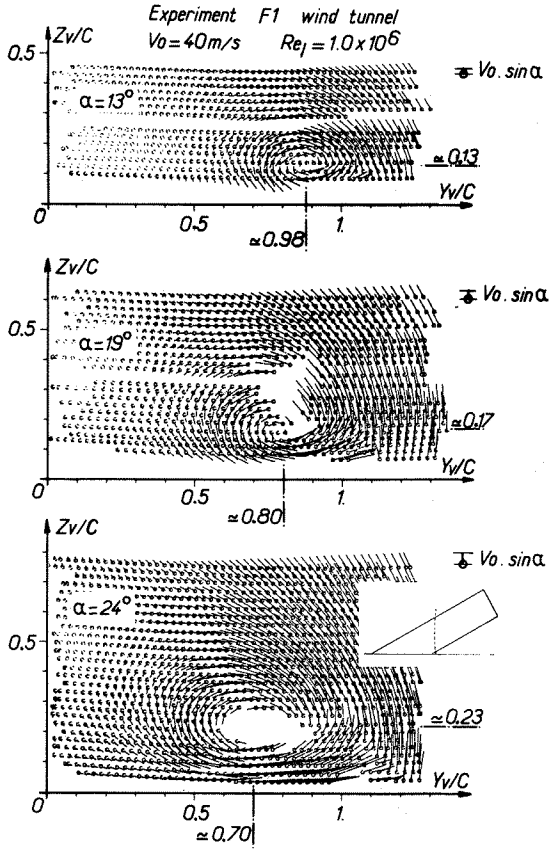

Fig. 5 - Planar view of measured velocity vector fields at various angles of attack.

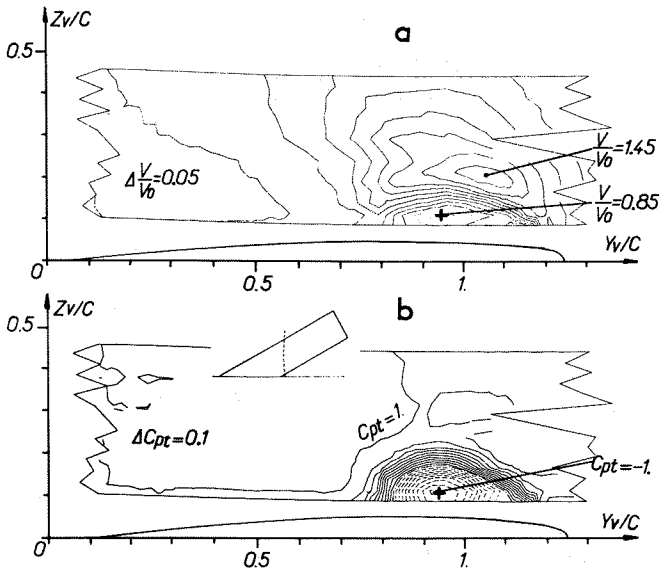

Fig. 6 - Probe survey results : α = 13°
a. velocity modulus contour lines.
b. total pressure contour lines.

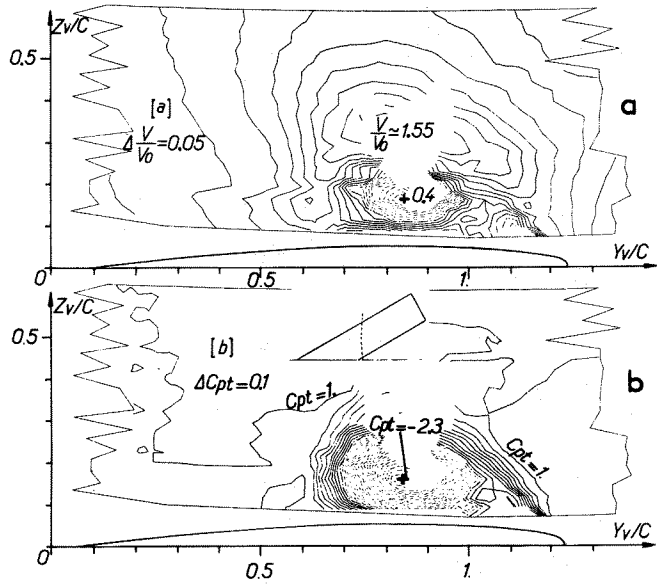

Fig. 7 - Probe survey results : α = 19°
a. velocity modulus contour lines.
b. total pressure contour lines.

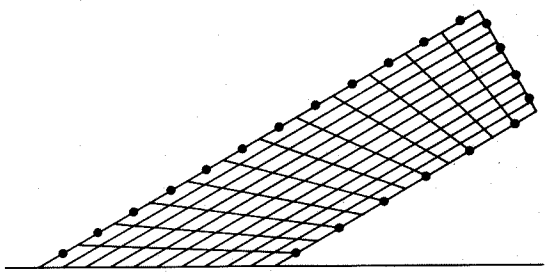

Fig. 8 - Wing panelling and vortex shedding point distribution.

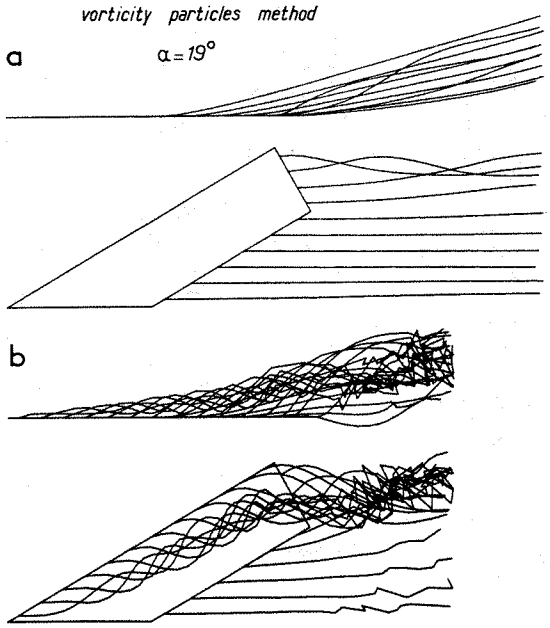

Fig. 9 - Computational emission lines
a. attached flow.
b. leading edge vortex flow.

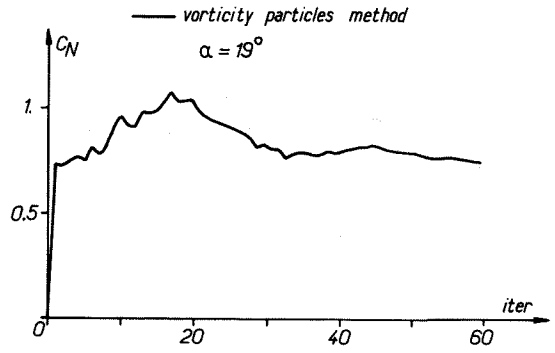

Fig. 10 - Leading edge vortex flow - Lift convergence.

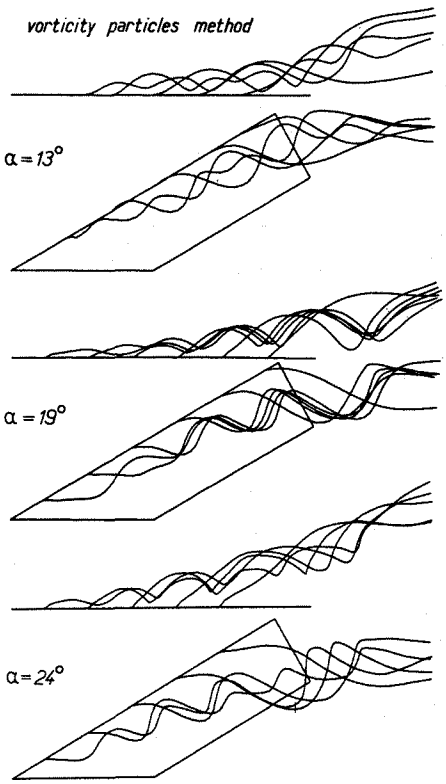

Fig. 11 - Leading edge vortex flow - Calculated streamlines at various angles of attack.

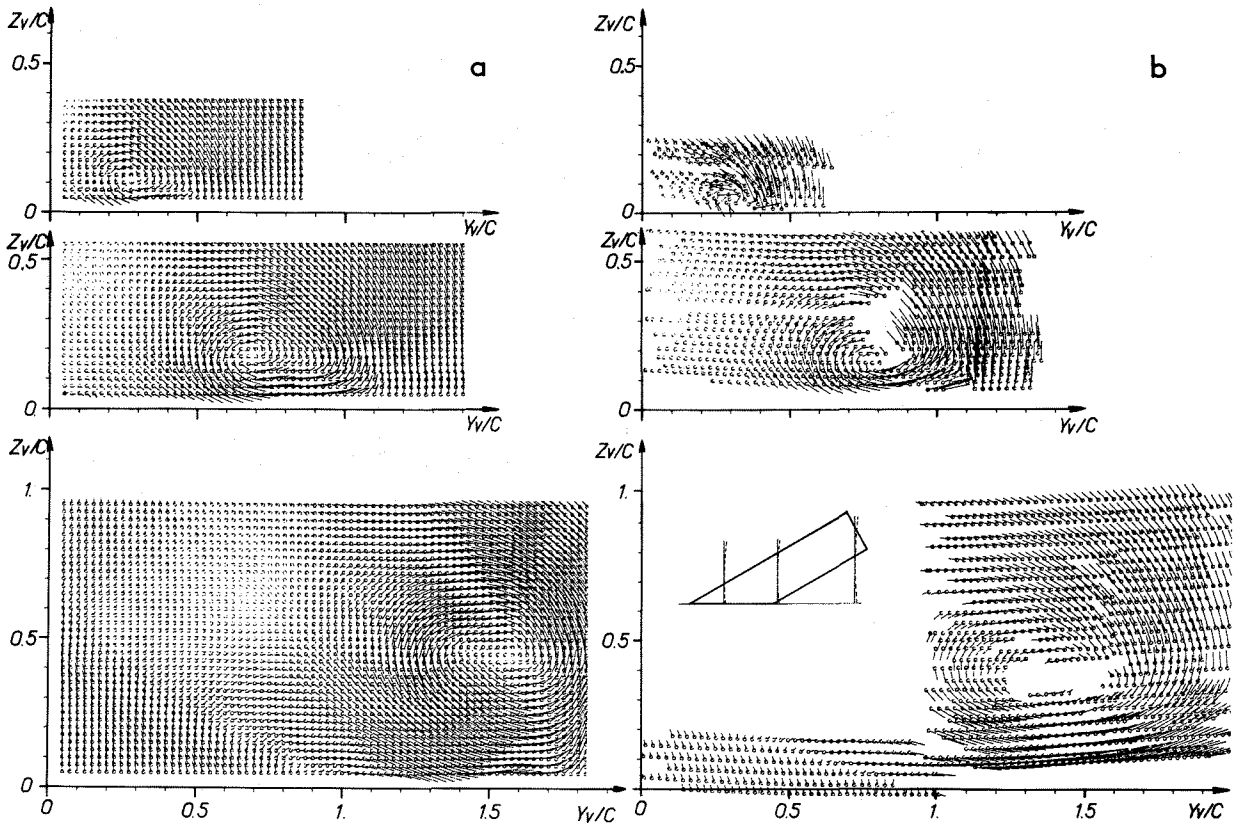

Fig. 12 - Planar view of the velocity vector field at $\alpha = 19°$
a. vorticity particles method.
b. experiment : F1 wind tunnel
(Vo = 40 m/s, Re$_\ell$ = 1.106).

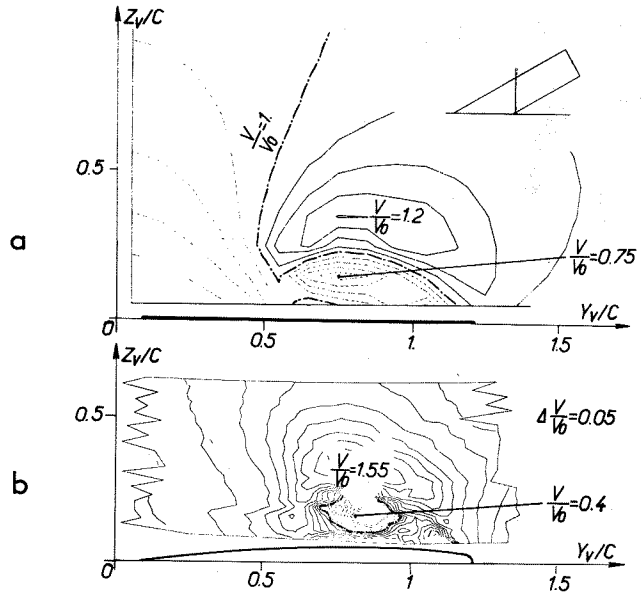

Fig. 13 - Velocity contour lines : α = 19°
a. vorticity particles method.
b. experiment : F1 wind tunnel (Vo = 40 m/s, Re_ℓ = 1.10⁶).

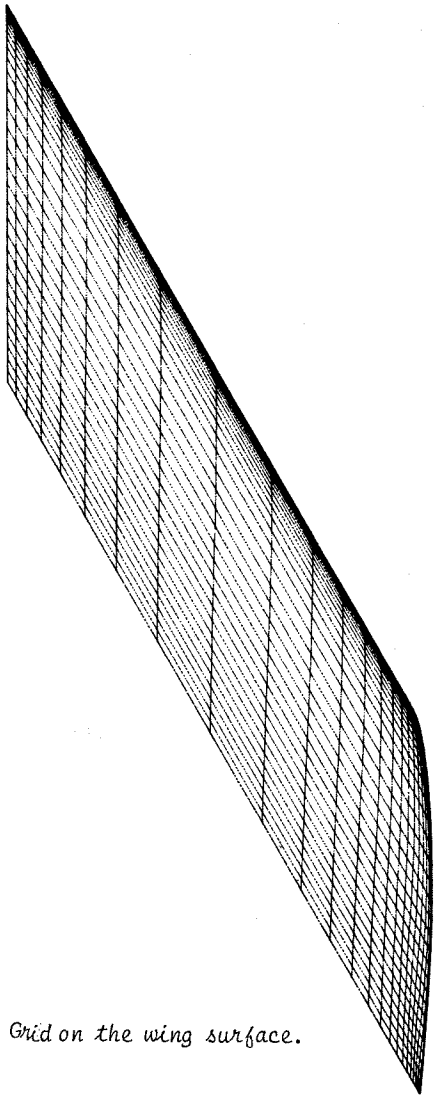

Fig. 15 - Grid on the wing surface.

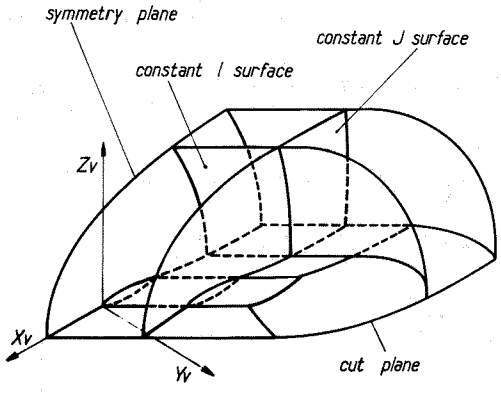

Fig. 14 - Grid sketch.

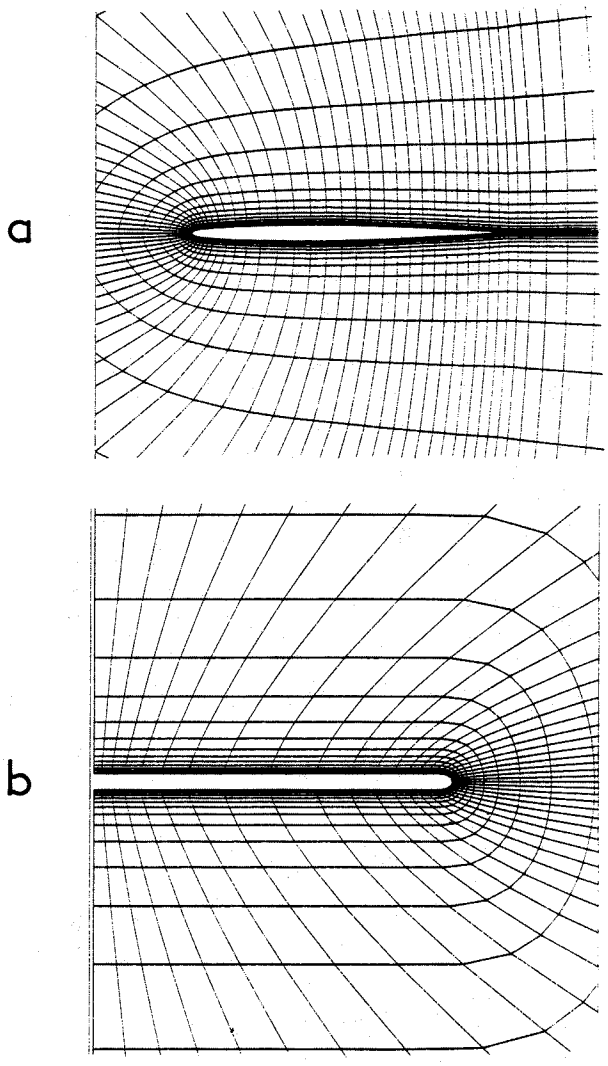

Fig. 16 - C-O type grid
a. C- type grid in the symmetry plane (y = o).
b. O- type grid on the surface (I = 18) (planar view in the x direction).

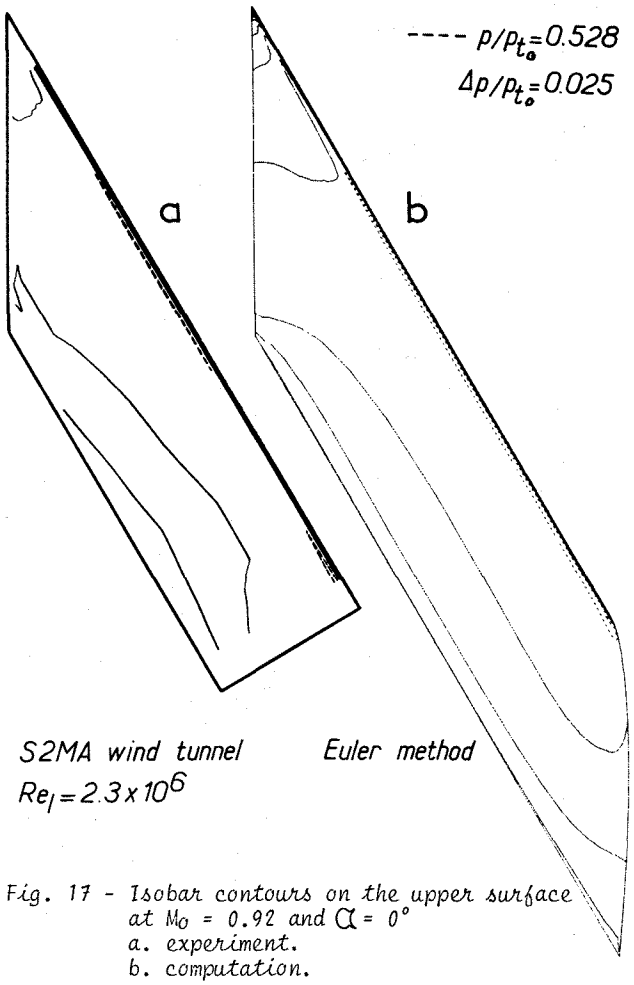

Fig. 17 - Isobar contours on the upper surface at M_o = 0.92 and α = 0°
a. experiment.
b. computation.

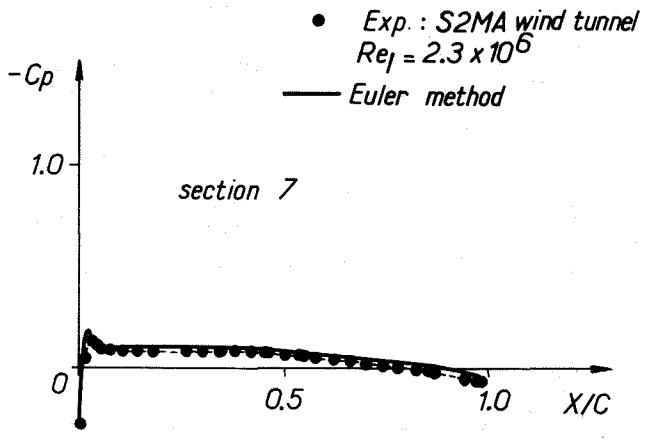

Fig. 18 - Pressure distribution on the wing in a mid-wing section at M_o = 0.92 and α = 0°.

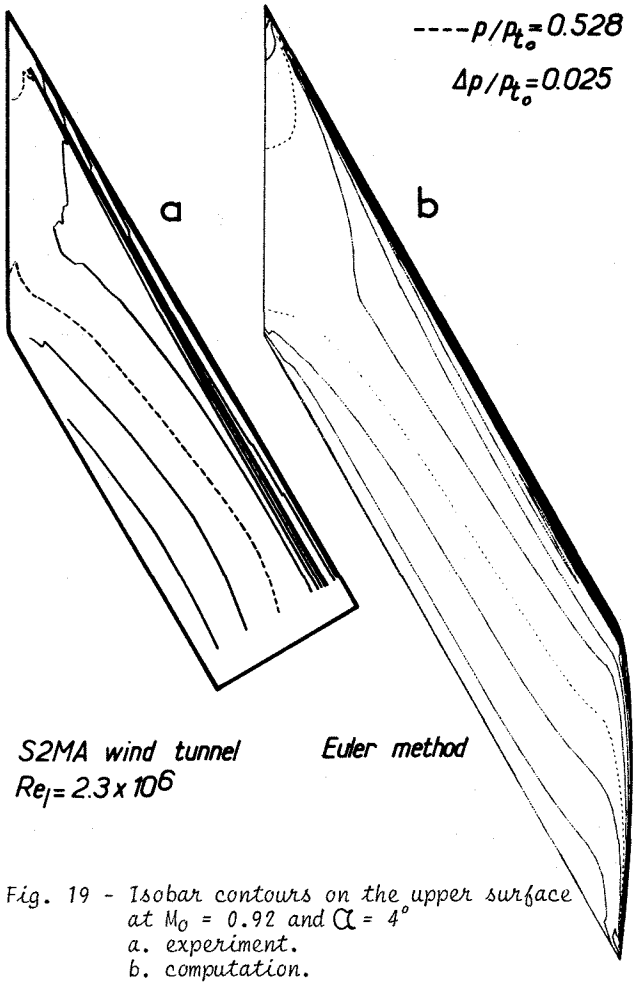

Fig. 19 - Isobar contours on the upper surface at M_o = 0.92 and α = 4°
a. experiment.
b. computation.

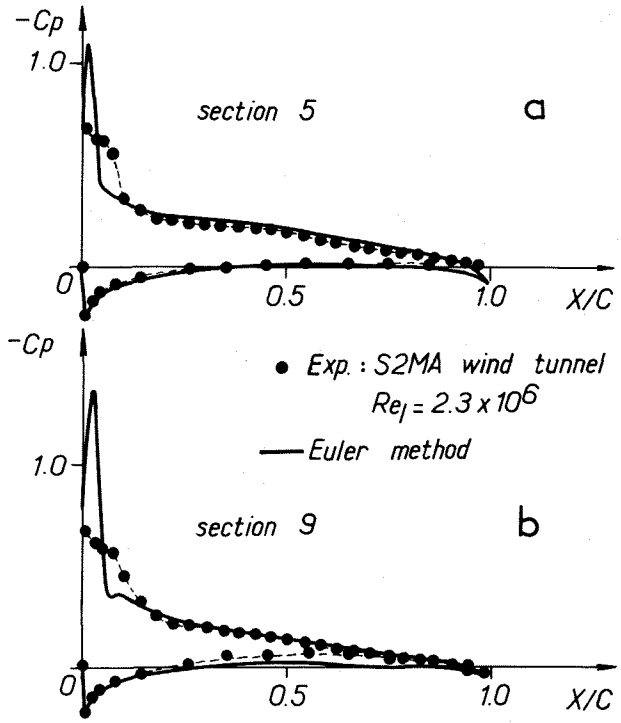

Fig. 20 - Pressure distributions on the wing at M_o = 0.92 and α = 4°
a. inner wing section.
b. outer wing section.

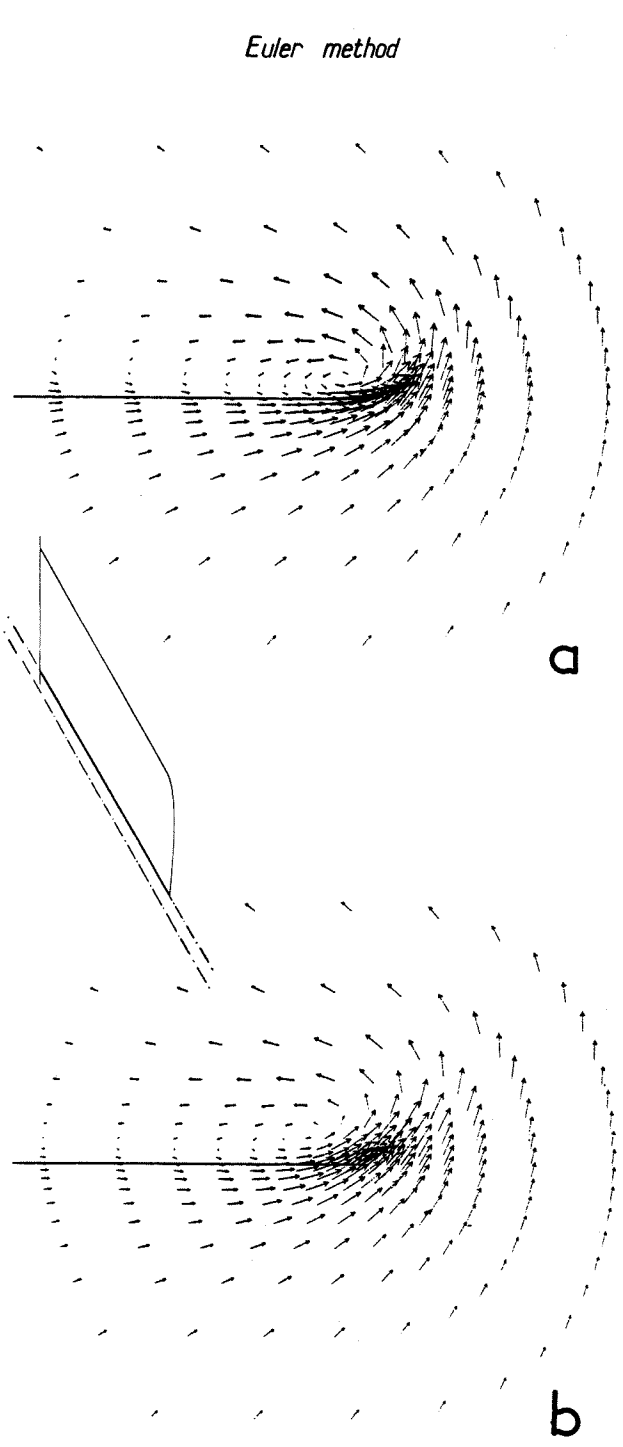

Fig. 21 - Velocity vector field on constant-I surfaces (planar view in the x direction) at $M_0 = 0.92$ and $\alpha = 4°$
a. at the trailing edge (I = 36).
b. downstream of the trailing edge (I = 42).

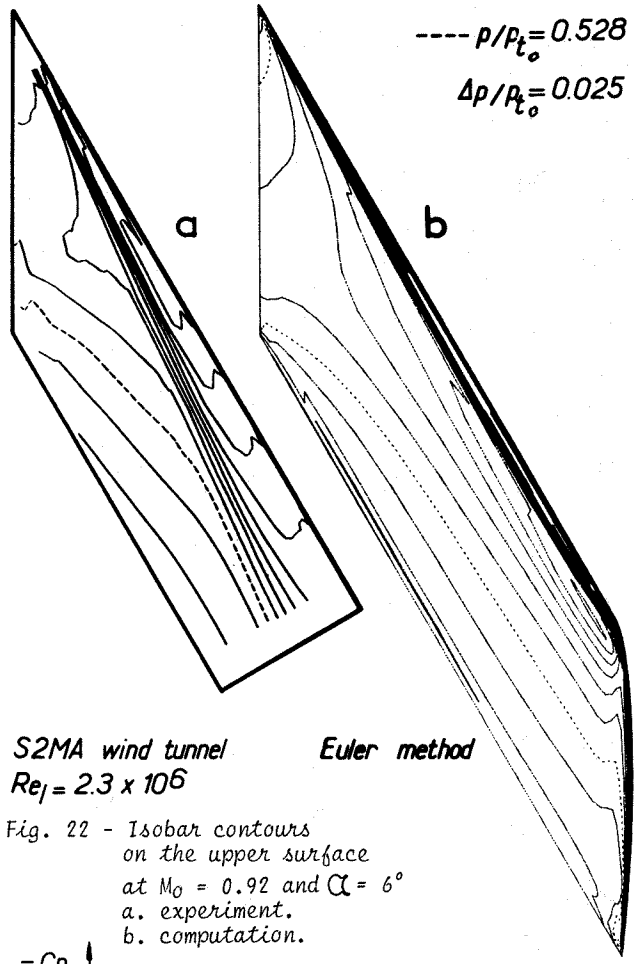

Fig. 22 - Isobar contours on the upper surface at $M_0 = 0.92$ and $\alpha = 6°$
a. experiment.
b. computation.

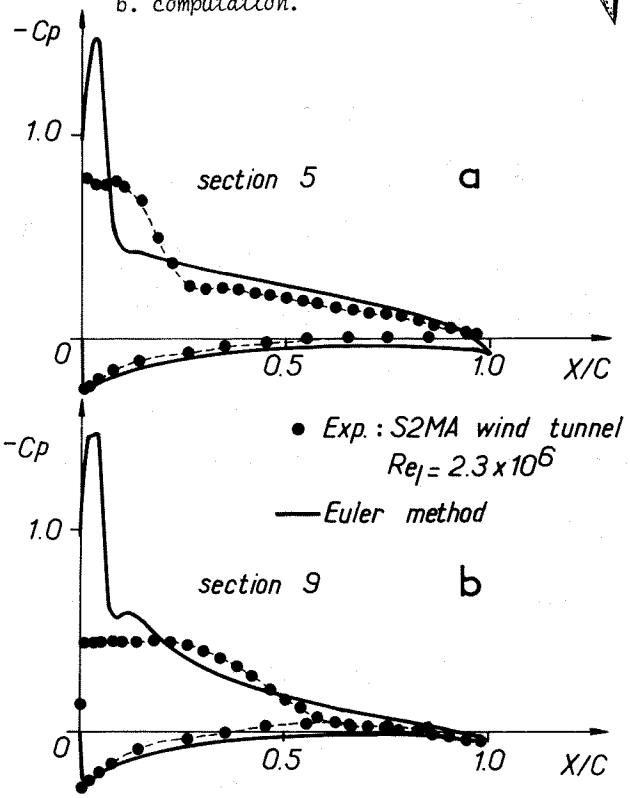

Fig. 23 - Pressure distributions on the wing at $M_0 = 0.92$ and $\alpha = 6°$
a. inner wing section.
b. outer wing section.

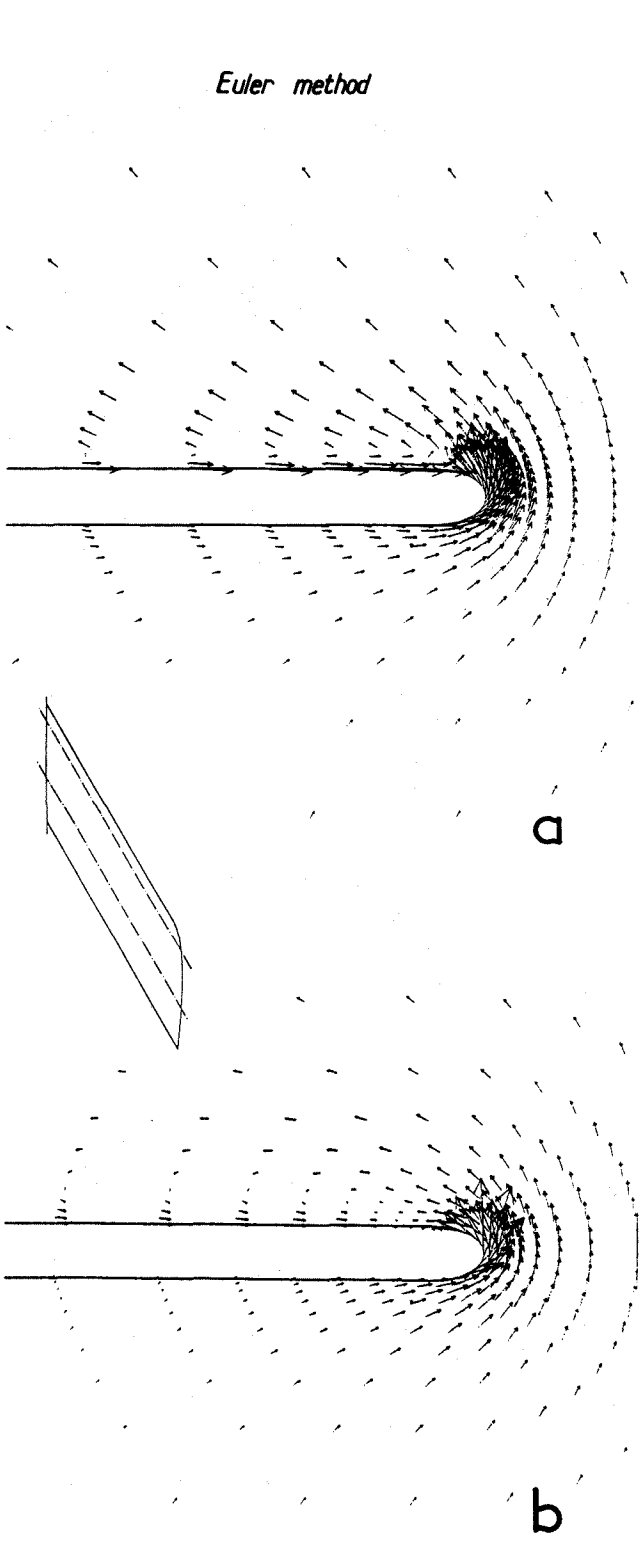

Fig. 24 - Calculated velocity vector fields on constant-I surfaces (planar view in the x direction) at $M_0 = 0.92$ and $\alpha = 6°$
a. downstream of the suction peak region (I = 15).
b. at mid-chord (I = 25).

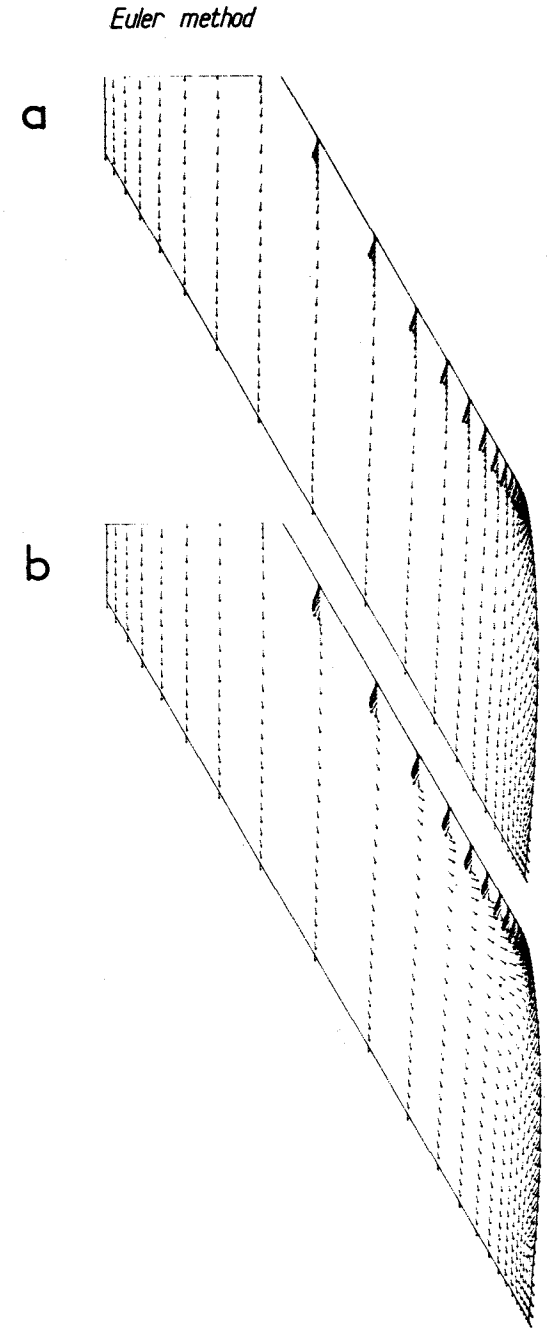

Fig. 25 - Calculated velocity vector fields on the upper wing surface at $M_0 = 0.92$
a. $\alpha = 4°$.
b. $\alpha = 6°$.

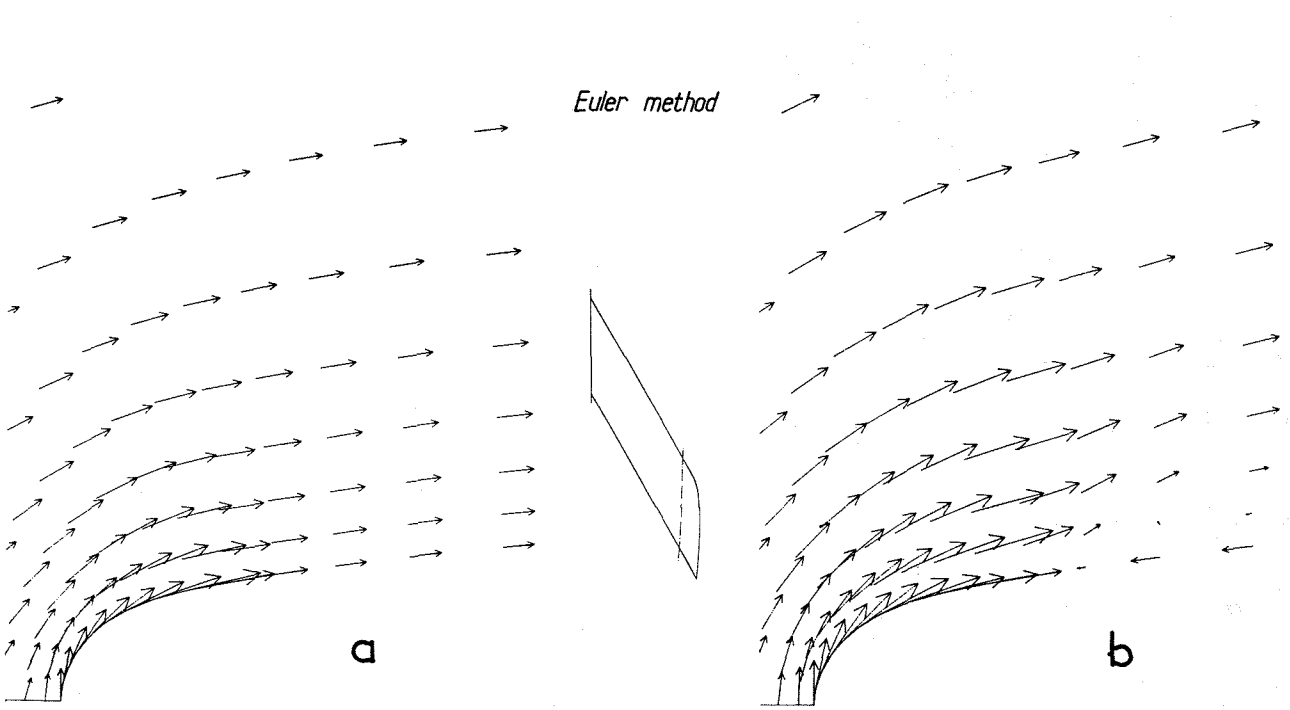

Fig. 26 - Calculated velocity vector fields on a constant J surface (J = 13 ; planar view in the leading and trailing edge direction) at $M_0 = 0.92$
a. $\alpha = 4°$.
b. $\alpha = 6°$.